Energy analysis of technologies to reduce electricity demand for heating in UK residential buildings

ACADEMIA GREEN ENERGY

Research Article
Published: 2025-12-22
https://doi.org/10.20935/AcadEnergy8057

Energy analysis of technologies to reduce electricity demand for heating in UK residential buildings

Sajan Preet[1,2,3,*], Stefan Thor Smith[2], Himanshu Saini[4]

Academic Editor: Aminhossein Jahanbin

Abstract

Residential buildings are among the largest consumers of electricity in the United Kingdom, with heat pumps representing a significant portion of this demand for space heating and domestic hot water. To encourage more flexible electricity usage, time-of-use (ToU) tariffs have been implemented, allowing consumers to adjust their energy consumption in response to daily fluctuations in electricity prices. Nevertheless, peak demand, which occurs during a limited number of hours, poses substantial challenges to the overall power balance and stability of the grid. As a result, there is increasing interest in deploying demand-side management (DSM) technologies to mitigate peak electricity demand for heating purposes. In this study, the effects of several DSM configurations were evaluated under cold climatic conditions, including photovoltaic panels paired with battery energy storage (PV–BESS, Case 1), PV–BESS combined with a solar thermal system (Case 2), and photovoltaic/thermal panels integrated with BESS (PV/T–BESS, Case 3). A simulation model of a typical UK residence, the David Wilson home, was developed in DesignBuilder/EnergyPlus to represent these scenarios and benchmark them against a baseline air-source heat pump setup (Case 0). For the winter month of January, simulations indicated that the heating-related electricity demand without any integrated technologies (Case 0) was 1531.6 kWh. This demand decreased to 1456.1 kWh in Case 1, 1318 kWh in Case 2, and 1132.47 kWh in Case 3. Among the configurations studied, the PV/T–BESS (Case 3) provided the largest reductions in both peak and total electricity demand, owing to its combined generation of electrical and thermal energy.

Keywords: *building electricity demand for heating, peak energy demand, battery energy storage system, solar-assisted heat pump, photovoltaic/thermal system*

Citation: Preet S, Smith ST, Saini H. Energy analysis of technologies to reduce electricity demand for heating in UK residential buildings. *Academia Green Energy* 2025;2. https://doi.org/10.20935/AcadEnergy8057

1. Introduction

The rapid growth of the global population, alongside rising living standards, has led to a substantial increase in energy demand worldwide [1]. Consequently, the energy consumption of buildings plays a critical role in shaping economic performance, energy generation requirements, and environmental outcomes in many countries [2]. The International Energy Agency [3] estimates that residential buildings account for approximately 32% of global energy use, with some nations reporting residential energy consumption surpassing that of industrial sectors [4].

In the United Kingdom (UK), domestic buildings contribute around 32.5% of total national energy use, of which nearly 68% is dedicated to space heating [5, 6]. Residential energy demand exhibits significant temporal variability, typically peaking in the morning and evening. The adoption of smart grid and microgrid systems has accelerated the shift from static to more dynamic energy consumption patterns [7]. Following the COVID-19 pandemic, both the magnitude and frequency of peak loads have increased due to more occupants spending extended periods in residential spaces [8].

Meeting peak electricity demand remains a critical challenge for energy providers. In the UK, the residential sector accounts for approximately 60% of maximum load, predominantly driven by heating requirements [9]. Traditionally, conventional power plants have been relied upon to satisfy this demand [10]. However, this approach is economically and environmentally unsustainable due to high fuel consumption, elevated maintenance costs, and increased carbon emissions [8]. During peak periods, electricity prices can rise to nearly eight times the off-peak rates [10]. Therefore, identifying strategies to curb peak energy demand while supporting the UK's net-zero targets has become an urgent research focus [11].

Demand-side management (DSM) has emerged as one of the most effective and sustainable solutions to alleviate peak energy demand in residential buildings [12]. DSM encompasses a variety of strategies, including energy-efficient technologies, dynamic pricing mechanisms, and demand–response programmes to manage both base and peak loads [13]. Time-based demand–response initiatives, such as time-of-use (TOU) pricing, critical peak pricing, and real-time pricing, have proven effective in reducing peak loads. In the UK, a three-tier TOU tariff system, known as TIDE or RAG, has been implemented. Under this scheme, electricity is billed at 6.41 pence per kilowatt-hour (p/kWh) during the off-peak period (23:00–06:00), increases to 29.99 p/kWh during the evening peak (16:00–19:00), and is charged at a standard rate of 14.02 p/kWh during all other hours (Green Energy UK).

[1]School of Chemical Engineering, University of Birmingham, Birmingham, UK.
[2]School of Built Environment, University of Reading, Reading, UK.
[3]Department of Mechanical Engineering, Regent College London, London, UK.
[4]Alliance for an Energy Efficient Economy, New Delhi, India.
*email: s.preet@bham.ac.uk

Beyond pricing strategies, DSM also integrates technologies such as energy-efficient appliances, distributed energy resources (DERs) including solar and wind generation [14], and energy storage systems, both electrical (EES) [15] and thermal (TES) [16]. This study investigates the impact of several DSM technologies, specifically solar-assisted heat pump systems, photovoltaic (PV) panels, photovoltaic/thermal (PV/T) systems, and battery energy storage systems (BESS), on peak electricity demand in residential buildings equipped with heat pumps under the UK's cold climatic conditions.

1.1. Literature review

Integrating solar thermal systems with heat pump configurations has been shown to enhance the Coefficient of Performance (COP), primarily because higher evaporator temperatures reduce the compressor workload compared with conventional heat pumps [17]. Ref. [18] conducted a parametric analysis of a solar-assisted heat pump system and demonstrated that enlarging the collector area and increasing the absorption coefficient substantially improved overall system performance. Similarly, ref. [19] optimised a solar-assisted heat pump for the mild winter conditions in Athens, evaluating various working fluids to maximise efficiency. Their study identified R32 as the most suitable refrigerant under steady-state conditions, followed by R1234yf. A 10 m^2 hybrid PV collector could provide 4.33 kW_{th} of thermal energy to the heat pump while simultaneously generating 0.53 kW_e of electricity.

Ref. [20] optimised a two-stage vapour-injected heat pump using R-32, R-290, R-410A, R-454A, and R-452B as working fluids. The system was modelled and simulated using the Non-dominated Sorting Genetic Algorithm II (NSGA-II) to generate Pareto-frontier curves. Results indicated that the system could achieve a maximum heating COP of approximately 5.2, while the minimum unit heating cost of around 0.19 USD/kWh was obtained with R-32 and R-290. The total operational cost ranged from 1.33 USD/h to 1.73 USD/h, corresponding to R-452B and R-290, respectively. Ref. [21] improved the thermal efficiency of an air-source heat pump by incorporating a novel refrigerant-heated radiator for thermal storage. In this setup, high-temperature refrigerant vapour from the compressor is directed to the radiator, which transfers heat to indoor spaces through radiation and natural convection. The study reported reduced heat losses and a uniform surface temperature. COP decreased from 4.4 to 3.5 when condensing temperatures rose from 35.9 °C to 44.0 °C, and from 4.2 to 1.8 as outdoor temperatures fell from 6.9 °C to −18.4 °C.

Battery energy storage systems (BESSs) are increasingly being deployed in residential buildings to store electricity generated by PV panels or purchased during off-peak periods, supporting heat pump operation during peak demand. Reference [15] found that 3 kW of battery storage per household allowed heat pumps to operate without imposing additional stress on substations during peak hours, corroborating the findings of [22]. Ref. [23] conducted simulations to determine optimal BESS sizing for residential buildings, suggesting typical capacities ranging from 5 kWh/2.6 kW for low electricity-demand homes to 22 kWh/5.2 kW for high-demand homes with electric space heating. Ref. [24] proposed a convex optimisation approach for electricity storage scheduling, considering tariffs and demand patterns. Ref. [25] reported that residential BESS investments could generally be recovered within three years, while [26] observed that installing 2–3 kWh batteries in apartments could reduce peak demand by up to 30%. More recently, ref. [27] concluded that integrating PV panels with BESS offers further energy savings, supporting the rationale for their combined use, as investigated in the present study.

1.1.1. Research gap and objective

Minimising electricity consumption for residential heating has become a key research priority due to its impact on grid stability, carbon emissions, and energy costs. In the United Kingdom, transitioning from conventional gas boilers to heat pump systems is a central approach for decarbonising domestic heating. However, several studies have highlighted that heat pumps can increase peak electricity demand relative to traditional boilers, potentially imposing additional stress on the grid infrastructure [11]. To address these challenges, a range of demand-side management (DSM) strategies have been investigated, including the deployment of photovoltaic (PV) panels and battery energy storage systems (BESSs). While prior research has largely examined solar-assisted heat pumps and BESSs separately, there is limited evidence regarding their combined effect on peak heating loads and overall energy consumption, particularly under cold-climate conditions. The present study seeks to address this gap by evaluating the performance of integrated DSM configurations in a representative UK residential building. Three configurations are considered: (i) PV–BESS (Case 1), (ii) PV–BESS integrated with a solar-assisted heat pump (Case 2), and (iii) photovoltaic/thermal (PV/T) panels combined with BESS (Case 3). These setups are compared against a baseline air-source heat pump system (Case 0) to assess their effectiveness in reducing both peak electricity demand for heating and total energy consumption during winter in the UK.

2. Materials and methods

This study investigates the effects of various demand-side management (DSM) technologies on reducing peak electricity demand for heating in residential buildings. The methodology is structured into three stages, as depicted in **Figure 1**. The first stage involves identifying the problem of elevated peak and overall energy demand, particularly during periods of high electric heating usage. In the second stage, a range of DSM strategies with the potential to alleviate this demand is examined, including on-site electricity generation technologies (PV panels and wind turbines), electrical energy storage systems (BESS), solar thermal systems, and photovoltaic/thermal (PV/T) systems. The third stage evaluates the thermal and energy performance of residential buildings incorporating these technologies and compares them against a baseline building configuration.

For the simulations, DesignBuilder Building Simulation software (version 7.3.1.003) was employed [28] to assess the potential of each technology in reducing peak energy demand. DesignBuilder is widely adopted for building energy analysis, offering detailed assessments of thermal performance, lighting, and overall energy consumption when integrating both active technologies and passive design measures [29]. The software also facilitates analyses of thermal comfort, environmental performance, and cost implications [30]. Additionally, it calculates solar heat gains while accounting for shading effects from surrounding structures across different months. Essential inputs, including material thermal properties, ventilation rates, and occupancy profiles, can be specified for defined time intervals. Hourly meteorological data from typical UK weather years were used to ensure simulation accuracy, as these datasets closely reflect real environmental conditions [31].

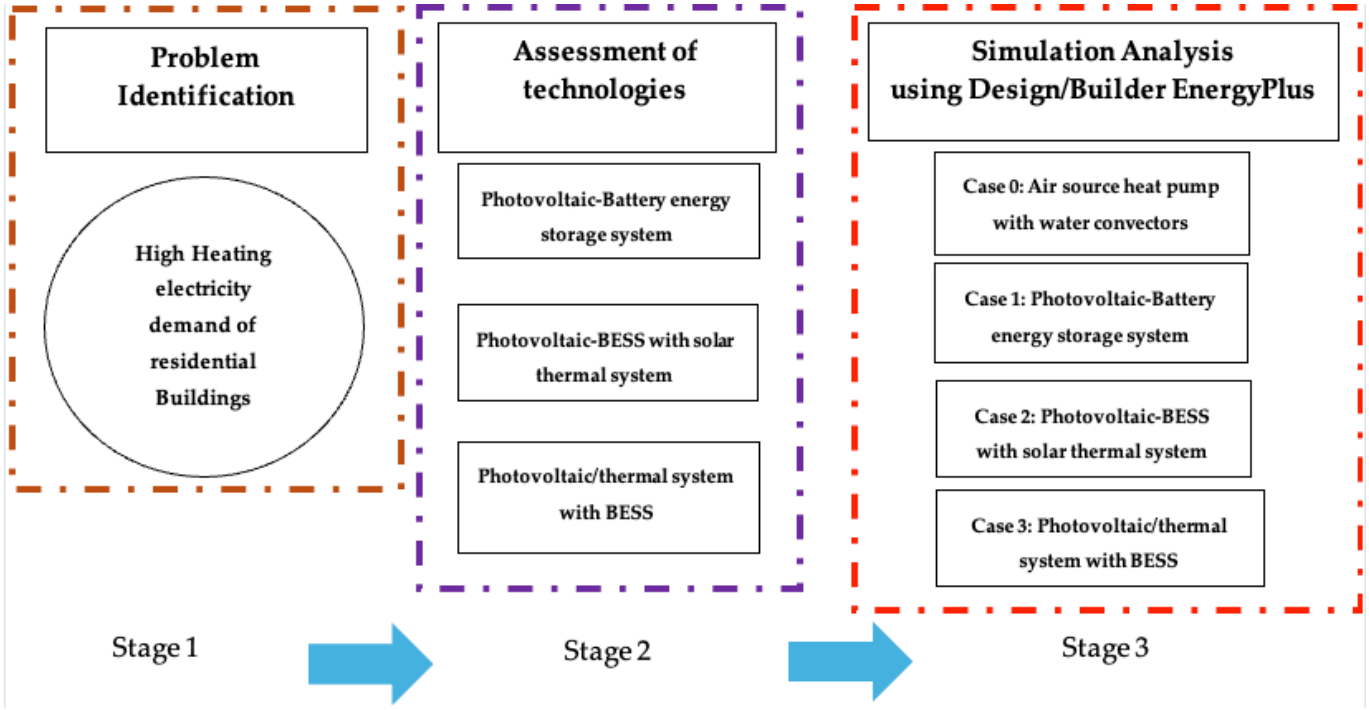

Figure 1 • Methodology flow chart in the present study.

2.1. Mathematical models of the components of residential heating systems

Ref. [11] developed an energy model of a heat pump system using the Finite Volume Method (FVM). This approach effectively captures the complex interactions between transient heat conduction and convective processes within heat pump components. By discretising the physical domain into smaller control volumes, the FVM allows for high spatial resolution, enabling detailed analysis of dynamic thermal and fluid behaviour, particularly in geometrically complex regions [32].

2.2. Energy modelling of the air-source heat pump system

The finite volume-based mathematical modelling of each component of the HP system is given below.

2.2.1. Water heater tank

A one-dimensional dynamic model of the water heater tank, based on the principles of mass, momentum, and energy conservation, was employed to analyse the behaviour of the sensible heat storage within the tank. The governing equations are expressed as follows:

$$\frac{\partial \rho}{\partial t} + \frac{\partial (\rho \nu)}{\partial x} = 0 \quad (1)$$

$$\frac{\partial (\rho A E)}{\partial t} + \frac{\partial (\rho A \nu)}{\partial x} = \frac{\partial (qA)}{\partial x} + \rho A g \frac{\partial z}{\partial x} + W \quad (2)$$

$$\frac{\partial (\rho \nu)}{\partial t} + \frac{\partial (\rho \nu^2)}{\partial x} = -\frac{\partial \rho}{\partial x} + \frac{\partial}{\partial x}\left(\mu \frac{\partial \nu}{\partial x}\right) \rho g \quad (3)$$

The variables used in the model are defined as follows: ρ denotes the fluid density, t represents time, and x specifies the spatial position. The fluid velocity along the x-axis is indicated by ν, while A corresponds to the cross-sectional area of flow. Total energy per unit mass is represented by E, and q denotes the heat flux. The height relative to a reference point is given by z, and W indicates the rate of work performed. Pressure is represented by p, dynamic viscosity by μ, and gravitational acceleration by g.

Figure 2 depicts the thermal storage tank, which is divided into N discrete control volumes along its vertical axis. Each control volume is analysed using a lumped modelling approach, assuming uniform temperature, density, and specific heat capacity within the volume [33]. For simplification, the system is considered under steady-state mass and momentum balance conditions. These assumptions are reasonable given the limited operating temperature range and the minimal influence of internal forces on the water temperature distribution [34]. Under these conditions, the governing equations are formulated to describe the energy and mass transfer within the ith control volume, enabling accurate estimation of temperature and energy dynamics in the storage tan.

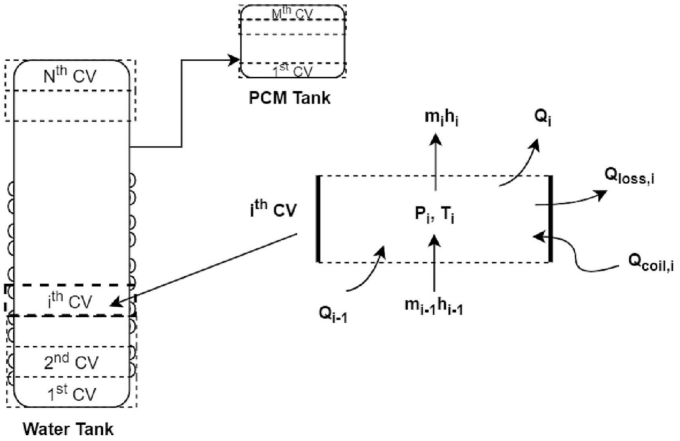

Figure 2 • Control volume schematic diagram of the water heater tank. Reproduced from [11].

$$0 = \dot{m}_{i-1} - m_i \tag{4}$$

$$m_i C_{p,\,i} \frac{dT_i}{dt} = (m_{i-1} H_{i-1} - m_i H_i) + Q_{coil,\,i} - Q_{loss,\,i} + (Q_{i-1} - Q_i) \tag{5}$$

$$0 = (p_i - p_{i+1}) + dp_{f,i} - \rho g z_i \tag{6}$$

where m is the mass flow rate (kg/s), C_p is the specific heat (kJ/kg K^{-1}), H is the specific enthalpy (KJ/kg), Q is the heat transfer rate (kW), p is the pressure (Pa), and Q_{loss} is the rate of heat loss from the tank to ambient temperature.

$$Q_{loss,\,i} = UA_i\,(T_i - T_a) \tag{7}$$

where T_a is the ambient temperature, UA_i is the overall heat transfer coefficient in ith control volume. It can be calculated using the equation

$$UA_i = \left(\frac{1}{\pi d_{int} L_i h_{int}} + \frac{\ln\left(\frac{d_{ext}}{d_{int}}\right)}{2\pi k L_i} + \frac{1}{\pi d_{ext} L_i h_{ext}} \right)^{-1} \tag{8}$$

where L_i is the tank height of the ith volume; d_{int}, d_{ext} is the inner and outer diameter of water tank; h_{int}, h_{out} is the convective heat transfer coefficient on inner and outer side, which is calculated as

$$\frac{h_{int} L_i}{k} = \begin{cases} 0.68 \times Pr^{0.5} \frac{Gr^{0.25}}{(0.952+Pr)^{0.5}} \; if\, 10 < GrPr < 10^8 \\ 0.13\,(PrGr)^{1/3} \; if\, GrPr > 10^9 \end{cases} \tag{9}$$

$$\frac{h_{ext} d_{ext}}{k} = Pr^{0.4} \left(0.4 Re^{0.5} + 0.06 Re^{2/3}\right) \left(\frac{\mu_\infty}{\mu_\omega}\right)^{0.25} \tag{10}$$

where k is the thermal conductivity, Gr is the Grashof number, Pr is the Prandtl number, Re is the Reynolds number, μ_∞ is the dynamic viscosity evaluated at the free stream temperature, μ_w is the dynamic viscosity calculated at wall temperature, and $Q_{i-1} - Q_i$ is the net rate of internal heat transfer of the ith control volume, which is evaluated as

$$Q_{i-1} - Q_i = \frac{k_i A}{\Delta x} (T_{i+1} - 2T_i + T_{i-1}) \tag{11}$$

where Δx is the control volume distance, A is the control volume cross sectional area, and k_i is the thermal conductivity of the ith control volume, which is calculated as

$$k_i = \begin{cases} k_i \times F \times |T_{i+1} - T_i| \; if\, T_{i+1} > T_i \\ k_i otherwise \end{cases} \tag{12}$$

where F is a parameter having a magnitude of higher order than k itself. When the temperature of control volume ith is higher than the temperature of control volume $(i+1)^{th}$, then thermal conductivity of the ith control volume pushes heat to transfer in an upward direction to resolve the temperature inversion.

Q_{coil} is the rate of heat transfer from the refrigerant to the water heater tank during the charging period, which is calculated as

$$Q_{coil} = m_r\,(H_{rin,\,i} - H_{rout,\,i}) \tag{13}$$

where m_r is the mass flow rate of the refrigerant, $H_{rin,\,i}$ and $H_{rout,i}$ are refrigerant enthalpies at the inlet and outlet of the ith control volume.

Total heat transfer between the Q_{coil} between the refrigerant and water tank is given by

$$Q_{coil} = \sum_{i=1}^{N} Q_{coil,\,i} = m_r\,(H_{rin} - H_{rout}) \tag{14}$$

where H_{rin} and H_{rout} are refrigerant enthalpies at the inlet and outlet of the condenser.

2.2.2. Compressor

To model the compressor, semiempirical modelling was adopted to predict its performance. The volumetric efficiency is determined as follows:

$$\eta_v \;=\; C_1 + C_2 \;\times \left(\frac{p_d}{p_s}\right)^{\frac{1}{\gamma}} \tag{15}$$

where p_s is the suction pressure of compressor, p_d is the discharge pressure of compressor, C_1 and C_2 are the constants having value 0.985 and −0.043, and γ is the isentropic exponent of 1.13.

The mass flow rate in the suction port of the compressor is given by

$$m_r = \eta_v \rho_s V_{disp} \tag{16}$$

The power of the compressor (W) is calculated as follows:

$$W \;=\; \left[C_3 \left(\frac{p_d}{p_s}\right)^{\frac{\gamma-1}{\gamma}} \;+\; C_4\right] \times p_s V_s \;+\; C_5 \tag{17}$$

where $C_3,\ C_4\ and\ C_5$ are the constants having values 10.31, −9.74, and 59.26, respectively.

Energy balance of the compressor is written as follows:

$$W \;=\; m_s\,(H_d - H_s) \;+\; Q_{loss} \tag{18}$$

H_s is the compressor suction enthalpy, H_d is the compressor discharge enthalpy, and Q_{loss} is the heat loss to the environment [35].

2.2.3. Evaporator

A transient evaporator model was developed to capture its dynamic thermal behaviour. In this approach, the evaporator is divided into multiple parallel circuits, and each circuit is further subdivided into several discrete segments. Each segment is treated as a two-fluid interaction zone where heat transfer occurs between the refrigerant and the air. As shown in **Figure 3**, this modelling strategy enables a detailed representation of the evaporator's heat exchange processes.

The mass, momentum, and energy balance equations are given below:

$$\frac{dM_{ref,\,i}}{dt} \;=\; m_{ref,\,i} - m_{ref,\,i+1} \tag{19}$$

$$\begin{aligned} \frac{d(U_{ref,\,i})}{dt} &= (m_{ref,\,i} H_{ref,\,i} - m_{ref,\,i+1} H_{ref,\,i+1}) \\ &+ \nu_{ref,\,i} A_c \left[(p_{ref,\,i+1} - p_{ref,\,i}) + \Delta p_{f,i}\right] \\ &+ h_{rw.ref} A_{suf}\,(T_{tw,i} - T_{ref,i}) \end{aligned} \tag{20}$$

$$\begin{aligned} \frac{d(m_{ref,i+1} L_{ref,i})}{dt} &= A_c\ (\rho_{ref,\,i} \nu_{ref,\,i} - \rho_{ref,\,i+1} \nu_{ref,\,i+1}) \\ &- A_c\,[(p_{ref,\,i} - p_{ref,\,i+1})] \\ &- A_c \Delta p_{f,i} - \rho_{ref,i} A_c g\,(z_{i+1} - z_i) \end{aligned} \tag{21}$$

The key parameters used in the model are described below. The refrigerant mass contained in the ith control volume is represented by $M_{ref,i}$, and its associated internal energy is indicated by $U_{ref,i}$. Each control volume has a segment length $L_{ref,i}$, and its vertical position is defined by the coordinates z_i and z_{i+1} for the i^{th} and $(i+1)^{th}$ segments, respectively. The flow passage has a cross-sectional area A_c, while A_{suf} denotes the overall heat transfer area provided by the tubes and fins of the evaporator. The heat

transfer between the tube wall and the refrigerant is governed by the convective coefficient $h_{\mathrm{tw,ref}}$. The friction-induced pressure drop across each segment is expressed as $\Delta p_{f,i}$.

At the inlet to each control volume, the refrigerant state is characterised by the mass flow rate $\dot{m}_{\mathrm{ref},i}$, enthalpy $H_{\mathrm{ref},i}$, pressure $p_{\mathrm{ref},i}$, density $\rho_{\mathrm{ref},i}$, and velocity $\nu_{\mathrm{ref},i}$. The temperature of the tube wall at the ith control volume is denoted by $T_{\mathrm{tw},i}$, while $T_{\mathrm{ref},i}$ represents the refrigerant temperature in the same segment.

In the two-phase section of the evaporator, the relative amounts of liquid and vapour refrigerant are determined through a void-fraction formulation applied along the pipe length. A simplified, lumped-parameter model is employed, allowing the void-fraction behaviour to be evaluated cumulatively from the beginning to the end of the evaporation region.

The void-fraction is calculated as

$$\nu f_i = \frac{\varepsilon_i}{[s_i u_i + \varepsilon_i (1 - s_i u_i)]} \tag{22}$$

Here, s_i denotes the slip ratio in the ith control volume, while ε_i and u_i represent the flow quality and the density ratio, respectively. These parameters are defined as follows:

$$\varepsilon_i = \frac{m_{vap,i}}{m_i} \tag{23}$$

$$u_i = \frac{\rho_{vap,i}}{\rho_{liq,i}} \tag{24}$$

In the ith segment of the model, m_i denotes the total mass flow of refrigerant, while the mass flow rate attributed to the vapour phase is written as $m_{\mathrm{vap},i}$. The corresponding vapour and liquid densities in this control volume are indicated by $\rho_{\mathrm{vap},i}$ and $\rho_{\mathrm{liq},i}$.

The air-side domain is analysed by applying the discrete forms of the mass, energy, and momentum conservation laws to each ith control volume. This process generates the governing equations that follow.

$$\frac{dM_{a,i}}{dt} = m_{a,i} - m_{a,i+1} + m_{cond,\,i} \tag{25}$$

$$\frac{dU_{a,i}}{dt} = m_{a,i}H_{a,i} - m_{a,i+1}H_{a,i+1} - m_{cond,\,i}H_{vap} + Q_{a,i} \tag{26}$$

$$0 = p_{a,i} - p_{a,i+1} - \Delta p_{a,i} \tag{27}$$

In the ith control volume, the air mass is denoted by $M_{a,i}$, and its internal energy is represented by $U_{a,i}$. At the entry of this control volume, the air flow is characterised by the mass flow rate $\dot{m}_{a,i}$, the enthalpy $H_{a,i}$, and the pressure $p_{a,i}$. At the exit, these parameters are expressed as $\dot{m}_{a,i+1}$, $H_{a,i+1}$, and $p_{a,i+1}$, respectively. Additionally, H_{vap} indicates the energy required for water vaporisation, while $\Delta p_{a,i}$ quantifies the pressure drop experienced by the air within the ith segment.

The rate at which water condenses, denoted by $\dot{m}_{\mathrm{cond},i}$, is obtained from the following expression:

$$m_{cond,i} = m_{a,i}w_{a,i} - m_{a,i+1}w_{a,i+1} \tag{28}$$

where $w_{a,i}$ and $w_{a,i+1}$ are the air humidity ratios at the inlet and outlet of the control volume.

The quantity $Q_{a,i}$ corresponds to the thermal energy exchanged between the air and the tube wall of the evaporator, calculated according to

$$Q_{a,i} = h_{da}A_{suf}(T_{tw,i} - T_{a,i}) \tag{29}$$

The parameter h_{da} corresponds to the convective heat transfer coefficient of dry air, and the temperatures of the air and the evaporator tube wall within the ith control volume are indicated by $T_{a,i}$ and $T_{tw,i}$, respectively.

For a wet wall surface, it is calculated as

$$Q_{a,i} = \frac{h_{wa}A_{suf}(H_{tw,i} - H_{a,i})}{C_{pa,i}} \tag{30}$$

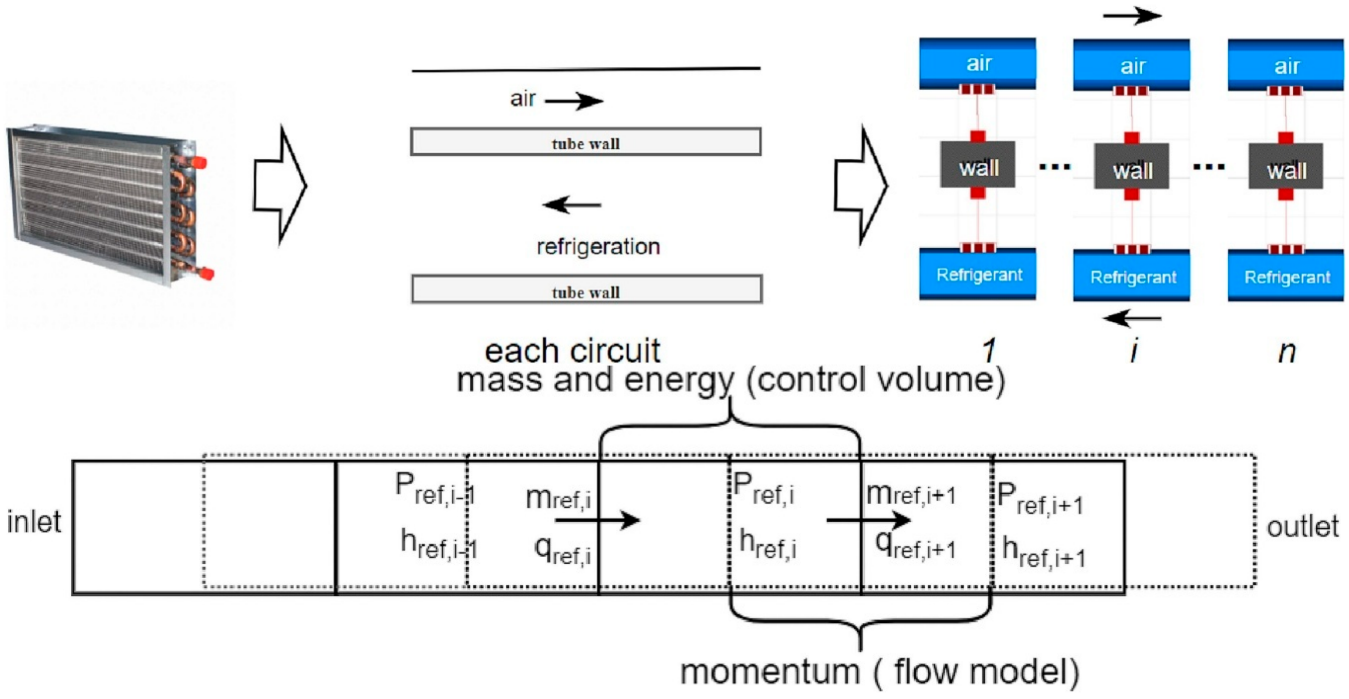

Figure 3 • Dynamic modelling of the evaporator of heat pump system. Reproduced from [11].

The convective heat transfer coefficient of dry air is given by

$$\frac{h_{da}D}{k} = \left(0.4Re^{0.5} + 0.06Re^{2/3}\right) Pr^{0.4} \left(\frac{\mu_\infty}{\mu_w}\right)^{0.25} \quad (31)$$

Here, D refers to the diameter of the pipe, k is the material's thermal conductivity, Re and Pr denote the Reynolds and Prandtl numbers, respectively, while μ_∞ and μ_w are the dynamic viscosities evaluated at the free-stream and wall temperatures.

The convective heat transfer coefficient of wet air is given by

$$h_{wa} = 0.73 \left(\frac{k^3 \rho^3 g}{\mu}\right)^{0.25} \left[\frac{1}{\Delta T \times D}\right]^{0.25} \quad (32)$$

$$m_{tw,i} C_{p,tw} \frac{dT_{tw,i}}{dt} = Q_{a,i} - Q_{ref,i} \quad (33)$$

Within the ith segment, the quantity $Q_{\text{ref},i}$ defines the convective energy exchange between the refrigerant and the tube wall, calculated according to

$$Q_{ref,i} = h_{tw,ref} A_{tw} \left(T_{tw,i} - T_{ref,i}\right) \quad (34)$$

In this context, $h_{tw,ref}$ defines the convective heat transfer coefficient between the evaporator tube wall and the refrigerant flow.

2.2.4. Expansion valve

The behaviour of the expansion valve is simulated using a semiempirical model, which ensures consistency with the compressor's mass flow. The expansion is considered an isenthalpic process, and the refrigerant mass flow rate is computed using the following relation:

$$m_v = C_v \sqrt{\rho_{in} \Delta p_v} \quad (35)$$

where C_v is the flow coefficient that can be a function of the valve opening;

$$C_v = K_1 + K_2 \times Pos + K_3 \times Pos^2 \quad (36)$$

where K_1, K_2, and K_3 are constants having values −0.78, 1.3, and 0, and Pos represents the valve position.

2.3. Energy modelling of the photovoltaic panel

The output power of the PV panel is calculated in EnergyPlus 8.9 using the equation below [36]:

$$Power_{PV} = \eta_{PV} \cdot G_T \cdot A_{PV} \quad (37)$$

where η_{PV} is the efficiency of the PV panel, G_T is the solar radiance incident on the tilted surface, and A_{PV} is the area of PV panel.

2.4. Energy modelling of the photovoltaic/thermal system

The *PV/T* thermal model, including the thermal and electrical outputs, is defined as

$$Thermal\ (Q)_{PV/T} = \eta_{th} \cdot G_T \cdot A_{PV/T} \quad (38)$$

$$Power_{PV/T} = \eta_{el} \cdot G_T \cdot A_{PV/T} \quad (39)$$

where η_{el} and η_{th} are the electrical and thermal efficiencies [37].

The energy balance of the battery energy storage system is defined as [38]

$$E_{t+1} = E_t + \eta_{ch} P_{ch} . \Delta t - \frac{P_{dis} \Delta t}{\eta_{dis}} \quad (40)$$

Subject to $0 \leq E_t \leq E_{max}$, where η_{ch} and η_{dis} are the charge and discharge efficiencies.

2.5. Energy modelling of the photovoltaic/thermal system

The useful thermal energy gain in the solar thermal collector is expressed as [37]

$$Q_u = A_c F_R \left[G_T (\tau\alpha) - U_L (T_i - T_a)\right] \quad (41)$$

where F_R is the collector heat removal factor, U_L is the overall heat loss coefficient, and T_i and T_a are the fluid inlet and ambient temperature, respectively.

2.6. System description and modelling

The modelling approach involved developing a detailed representation of a residential building and its integrated energy systems, including a heat pump, solar photovoltaic (PV) panels, solar thermal collectors, photovoltaic/thermal (PV/T) systems, and battery storage units. These simulations were conducted using DesignBuilder and EnergyPlus software. **Figure 4** shows the selected case study: a David Wilson home located at the University of Nottingham. This two-storey dwelling measures 7.9 m × 7.9 m × 5.0 m, with a total floor area of 62.41 m^2. The model incorporates construction materials matching the actual building, and the simulations use a London weather file. The building is designed to represent a family of four (two working adults and two children), with occupancy, heating demand, lighting, hot water use, ventilation, and appliance loads configured to reflect realistic household behaviour.

Figure 5 depicts the simulation model, including glazing and construction materials. The thermal transmittance (U-values) assigned to building components are external walls, 0.22 W/m^2·K; roof, 0.19 W/m^2·K; glazing, 1.8 W/m^2·K; doors, 2.2 W/m^2·K; and floor, 0.2 W/m^2·K. Occupancy, heating, hot water, and appliance profiles were constructed to reflect real-life conditions, with different patterns for weekdays and weekends. On weekdays, residents leave the house at 7:30 a.m. and return at 6:00 p.m., while on weekends all occupants remain at home. Internal heat gains per occupant are set at 90 W (sensible) and 60 W (latent), while appliance heat gains are maintained at approximately 530 W. Lighting and appliance use follows the occupancy schedule, excluding sleeping hours. Heating set-points follow CIBSE guidelines [39]: bedrooms are maintained at 18 °C overnight (10:00 p.m.–5:30 a.m.), reduced to 15 °C during unoccupied weekday hours, and maintained at 21 °C at other times. The PV panels are installed on the roof of the David Wilson EcoHome, a demonstration site for sustainable residential energy technologies at the University of Nottingham. The location receives an average annual solar irradiation of approximately 1000–1100 kWh/m^2/year, supporting the simulation of integrated PV, PV/T, and battery systems for energy demand analysis.

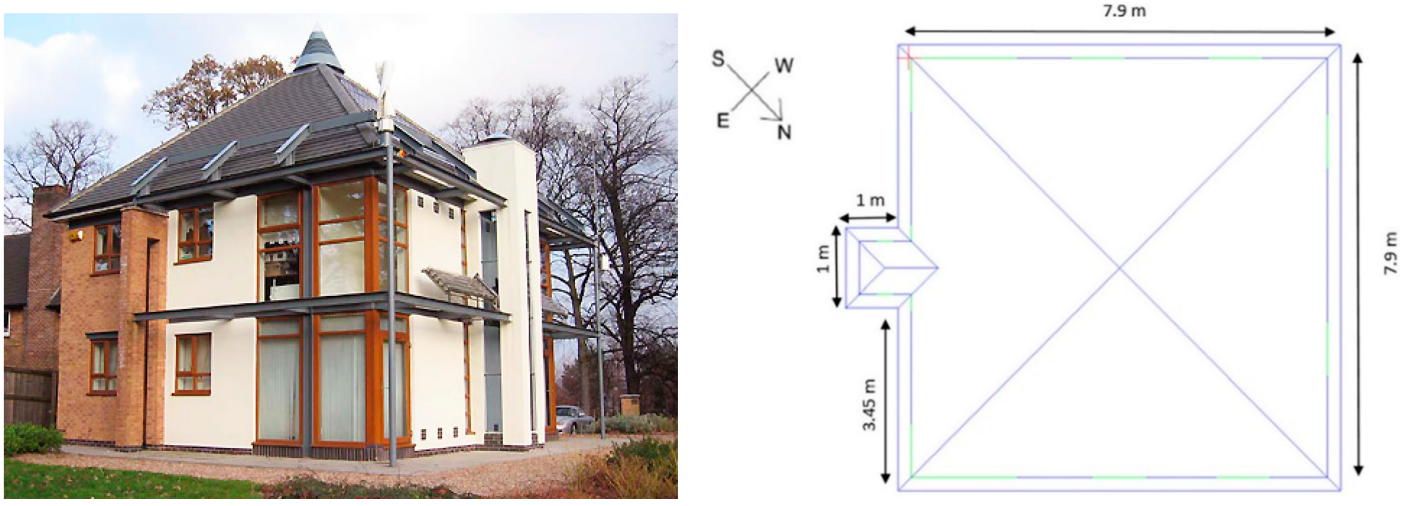

Figure 4 • David Wilson home (**a**) located at the University of Nottingham and layout (**b**).

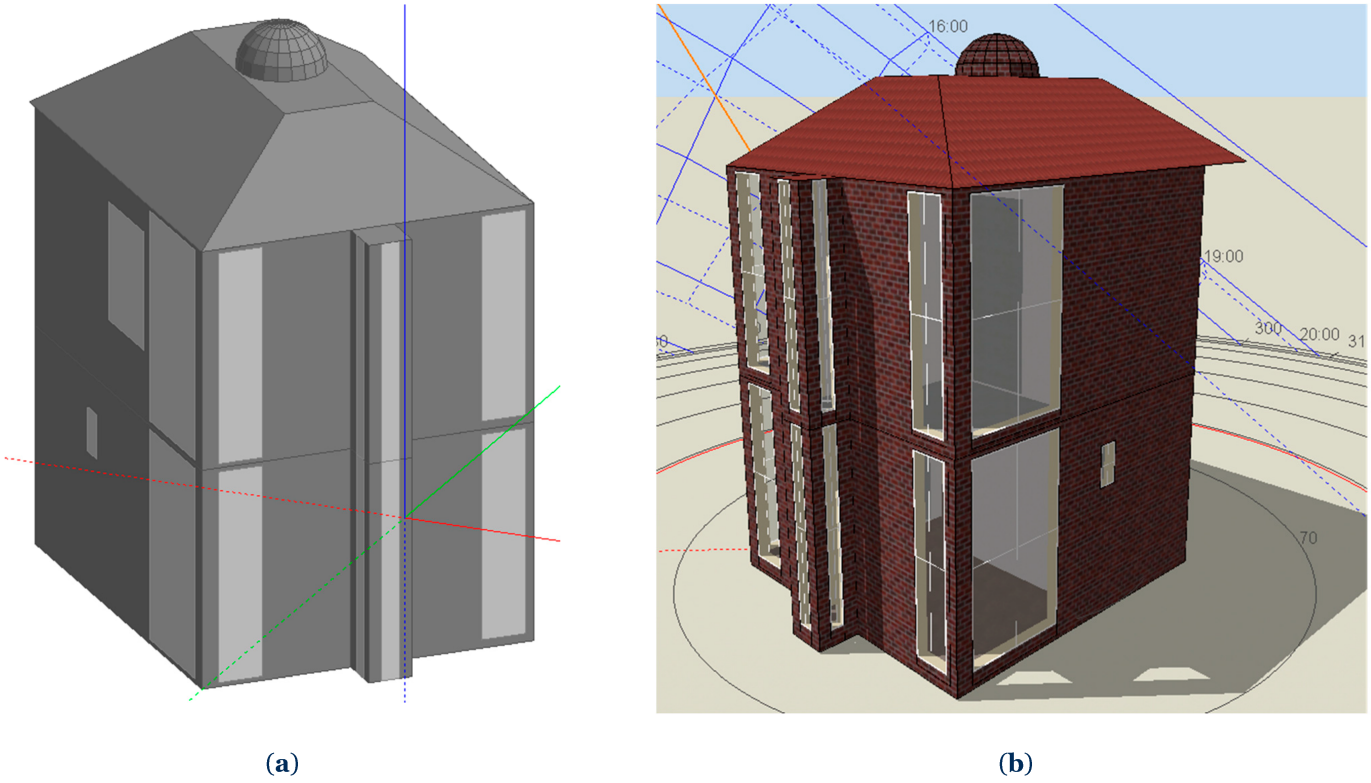

Figure 5 • Simulation model of the David Wilson home. Model view (**a**), Rendered View (**b**)

In this study, three distinct Energy Management Strategies (EMSs) were developed and analysed to optimise the operation of the heat pump (HP) system integrated with different renewable configurations. These strategies were designed to evaluate how the integration of photovoltaic (PV), photovoltaic–thermal (PVT), and solar thermal systems with a battery energy storage system (BESS) influences overall energy performance of a heating system.

- EMS–1: PV–BESS

In this configuration, the electricity generated by PV panels are stored in BESSs for later use. The EMS prioritises self-consumption of PV energy and minimises grid import by charging the battery during high irradiance periods and discharging it during evening demand peaks. The heat pump operates in accordance with heating demand, utilising grid support when PV generation is insufficient.

- EMS–2: PV–BESS with Solar Thermal System

This strategy integrates a separate solar thermal collector alongside the PV array. The EMS coordinates between electrical and thermal inputs where solar thermal energy directly contributes to meeting heating demand, thereby reducing the operating hours and electrical load of the heat pump. The BESS continues to provide load balancing for PV-generated electricity. This hybrid approach enhances system resilience and improves renewable utilisation by combining direct solar heating with stored electrical energy.

- EMS–3: PVT–BESS

The third configuration employs a photovoltaic–thermal (PVT) system that simultaneously generates electricity and heat. The EMS governs both electrical and thermal flows, optimising PVT operation to maximise overall system efficiency. Electrical energy powers the heat pump and PV panels charge the BESS, while recovered thermal energy preheats the heat pump's evaporator or supports the domestic hot water circuit. This integrated control reduces electricity consumption and enhances system COP under varying climatic conditions.

The technical specifications of the PV, PVT, and BESS components are given in **Table 1**. The battery energy storage system (BESS) integrated with the PV system has a rated power output of 3 kW and an energy capacity of 6 kWh, providing approximately 2 h of full-load discharge. The battery capacity was selected based on the building's daily electricity consumption to optimise self-consumption of PV-generated electricity during periods of low solar availability. The PV array is mounted on a south-facing roof with an installed capacity of 4 kWp, covering approximately 22 m^2, assuming a panel efficiency of 18%. The system was designed to supply around 35–40% of the building's annual electrical demand, considering the site's solar potential and the measured load profile of the David Wilson EcoHome.

Photovoltaic–thermal (PVT) collectors are integrated alongside the PV array to provide both electrical and thermal energy for space heating and domestic hot water (DHW). The installed PVT system has a rated electrical capacity of 3 kWp and a collector area of approximately 22 m^2. The sizing of the PVT collectors was determined using an energy balance and demand-matching approach, considering the building's thermal load, local climatic conditions, and the operating parameters of the heat pump system. Overall, the sizing of the PV, PVT, and BESS components was based on a demand-oriented design process using site-specific meteorological data, monitored building loads, and operational performance targets. This ensures that the proposed configuration is technically feasible, energy-efficient, and reproducible for similar residential applications.

In Case 1, PV panels are installed on the rooftop of the David Wilson residential building to generate on-site electricity, which is stored in the 3 kW battery system, following the recommendation of [15]. In Case 2, PV panels and solar thermal collectors are separately mounted on the roof. Electricity generated by the PV panels is stored in the batteries, reducing the building's total energy consumption, while hot water produced by the solar thermal collectors is transferred to a storage tank integrated with the air-source heat pump (ASHP), as shown in **Figure 6**, enhancing the system's coefficient of performance (COP). In Case 3, a PVT system is installed on the roof, generating both electricity and hot water simultaneously. The thermal energy recovered from the PVT modules is stored in a water tank, contributing to an improved overall system COP [40]. The performance improvement of the PVT system arises not from a larger collector area but from its integrated design, which enables efficient use of the absorbed solar energy for both electrical generation and heat recovery. This synergistic effect leads to higher combined thermal and electrical outputs compared with separate PV and solar thermal systems installed under similar conditions [37].

Table 1 • Technical specifications of PV, PVT, and BESS components.

Components	Rater power/capacity	Area/size (m^2)	Efficiency	Orientation	Notes
PV panels	4 kWp	22	18%	South facing, 30° tilt	Supplies ~35–40% of annual electricity demand
Solar collector	-	22		South facing, 30° tilt	Provides thermal energy for heating
PVT collectors	3 kWp (electrical)	22	18% electrical, ~50% thermal	South facing, 30° tilt	Provides both electricity and thermal energy for heating
Battery (BESS)	3 kW/6 kWh	N/A	Round-trip efficiency ~90%	N/A	Provides ~2 h of full-load storage; prioritises PV self-consumption

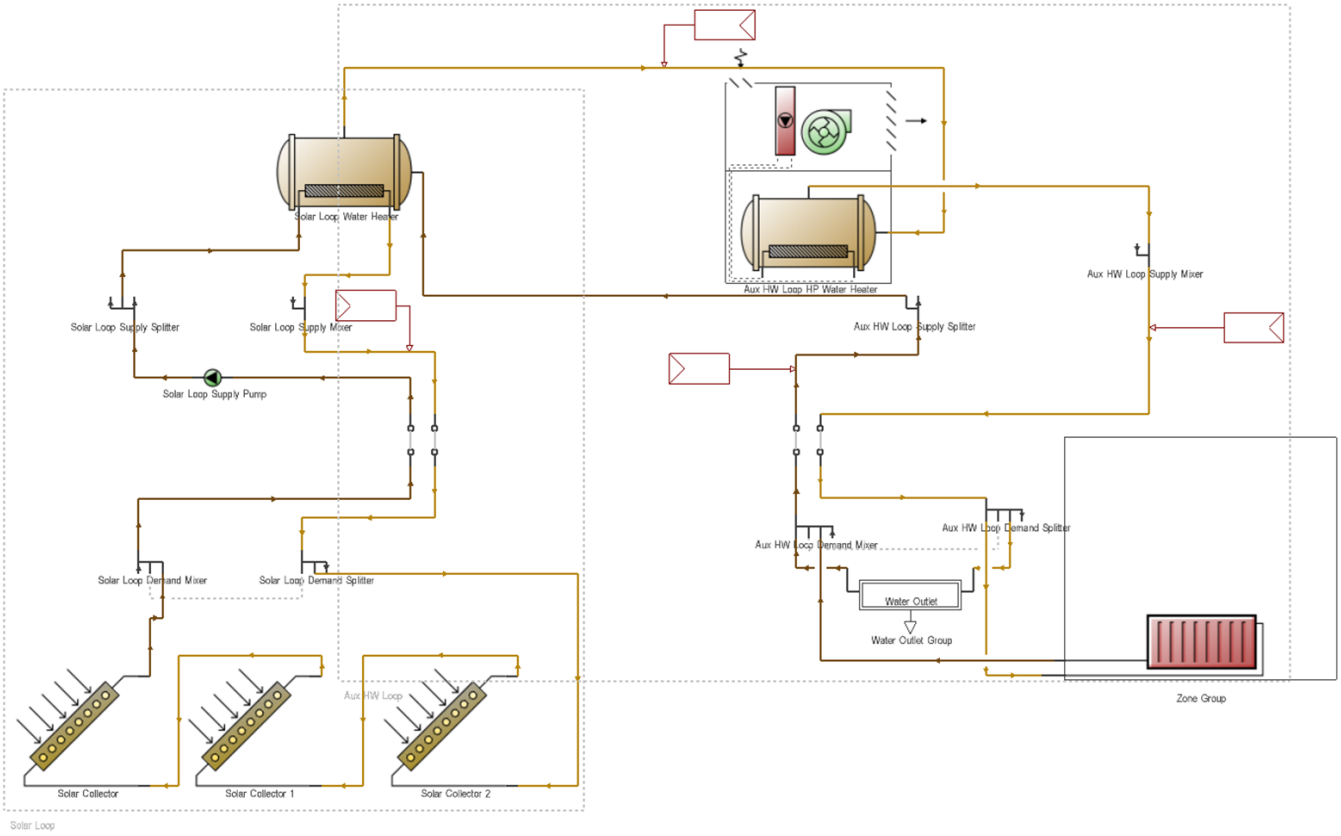

Figure 6 • Detailed schematic diagram of solar-assisted heat pump components with water convectors.

3. Results and discussion

3.1. Heating and electricity demand of the residential building

The building's heating load for January was evaluated using DesignBuilder/EnergyPlus. **Figure 7a,b** present the variation in ambient temperature, wind speed, and solar radiation in London over a representative 10-day period. Under typical London climatic conditions, the average dry-bulb temperature during January is approximately 2 °C. **Figure 8a** presents the hourly heating demand profile of the residential building in the base-case model, while **Figure 8b** highlights thermostat-controlled peaks corresponding to morning and evening occupancy hours. The peak hourly heating demand is estimated at approximately 15 kW, with the total heating energy demand for January reaching 1531.68 kWh (**Figure 9**). For comparison, ref. [16] reported a monthly heating demand of 1498 kWh for the David Wilson home; however, their study did not consider domestic hot water (DHW) demand. The baseline ASHP in the current study exhibited an average COP of 3.5, corresponding to a seasonal COP (SCOP) of 3.6 under UK winter conditions. When including electricity consumption for lighting, fans, and other appliances, the total energy demand of the base-case model is 2452.61 kWh (**Figure 10**).

In Case 1, the integration of a rooftop photovoltaic (PV) array with a 3 kW battery energy storage system (BESS) was intended to reduce grid dependency during peak heating periods. The PV panels generated 75.53 kWh of electricity, leading to a reduction in total electricity demand for heating to 1456.15 kWh (**Figure 9**) and a corresponding decrease in total energy consumption to 2376.56 kWh (**Figure 10**). This reduction of approximately 5% compared with the base case aligns with the findings of ref. [15], who demonstrated that small-scale PV–BESSs can effectively shift electrical loads and enhance energy flexibility in domestic buildings.

In Case 2, the system configuration was extended to include a solar thermal collector integrated with the ASHP, in addition to the PV–BESS arrangement. This setup achieved a further reduction in peak electricity demand for heating to approximately 12 kW (**Figure 9**). The solar thermal collectors preheated the ASHP's source water, reducing compressor operation and improving performance under cold conditions. As a result, the heating electricity demand decreased to 1393.52 kWh, and with supplementary PV generation, the ASHP's consumption further declined to 1318 kWh. The effective SCOP increased to 3.9, indicating improved seasonal efficiency due to a lower temperature lift across the compressor and a more stable source temperature. The overall monthly energy demand was reduced to 2223.81 kWh (**Figure 9** and **Figure 10**), representing a 9% improvement relative to the base case. The reduction in fan energy consumption (142.98 kWh) also indicates enhanced heat transfer efficiency. These outcomes are consistent with the work of refs. [40, 41], who observed that hybrid PV–thermal–heat pump configurations can improve system stability and COP during winter operation. However, this configuration introduces greater system complexity and higher upfront cost, which may constrain its adoption in small-scale residential applications.

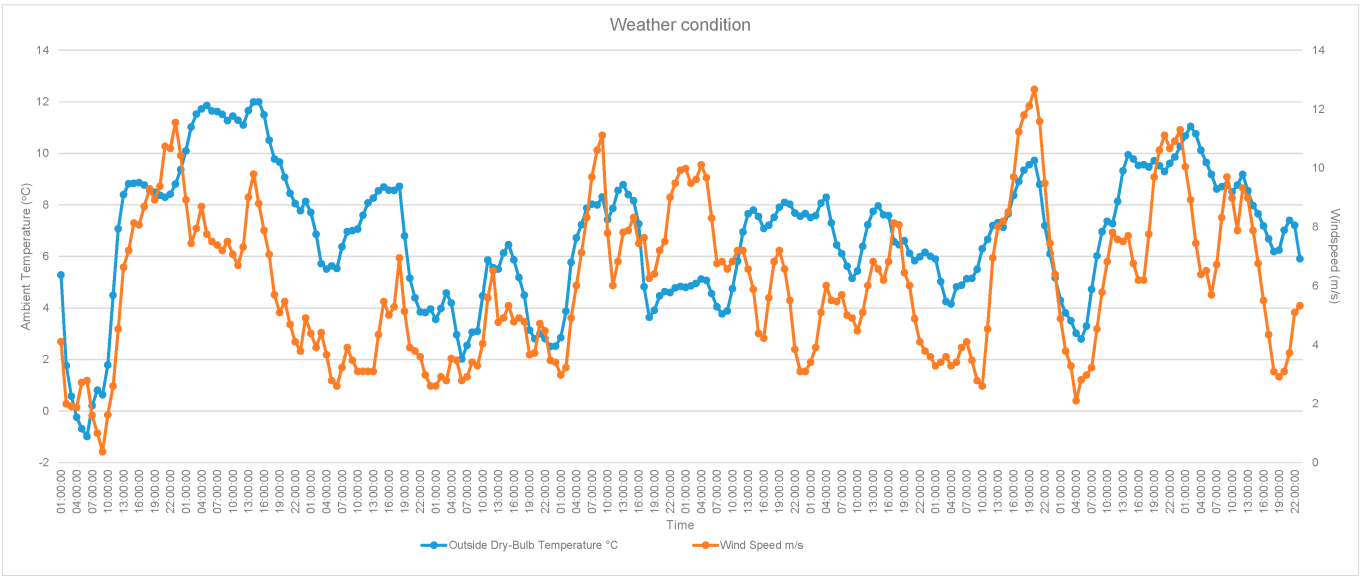

(**a**)

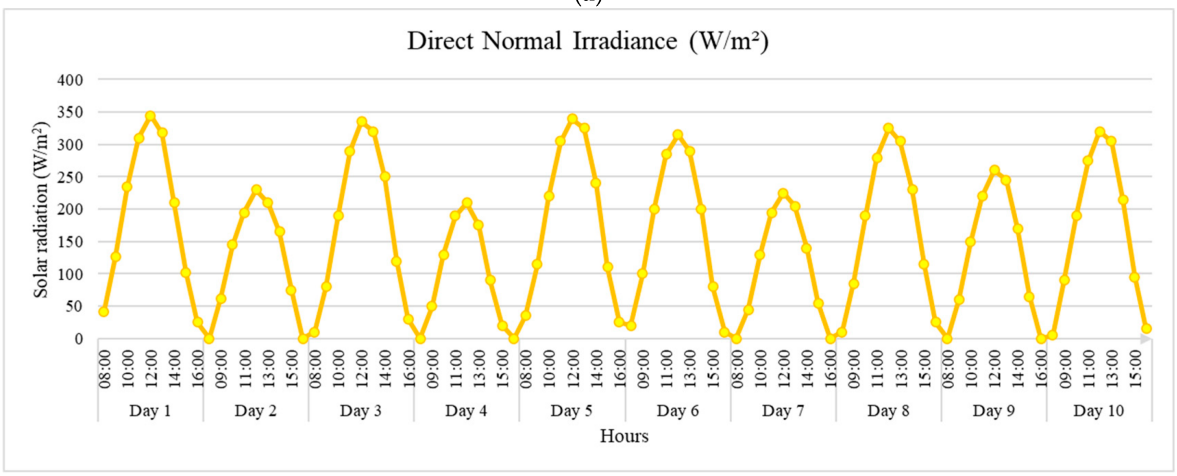

(**b**)

Figure 7 • (**a**) Ambient temperature and wind speed for 10 days in January; (**b**) hourly solar radiation data for a 10-day winter period in January.

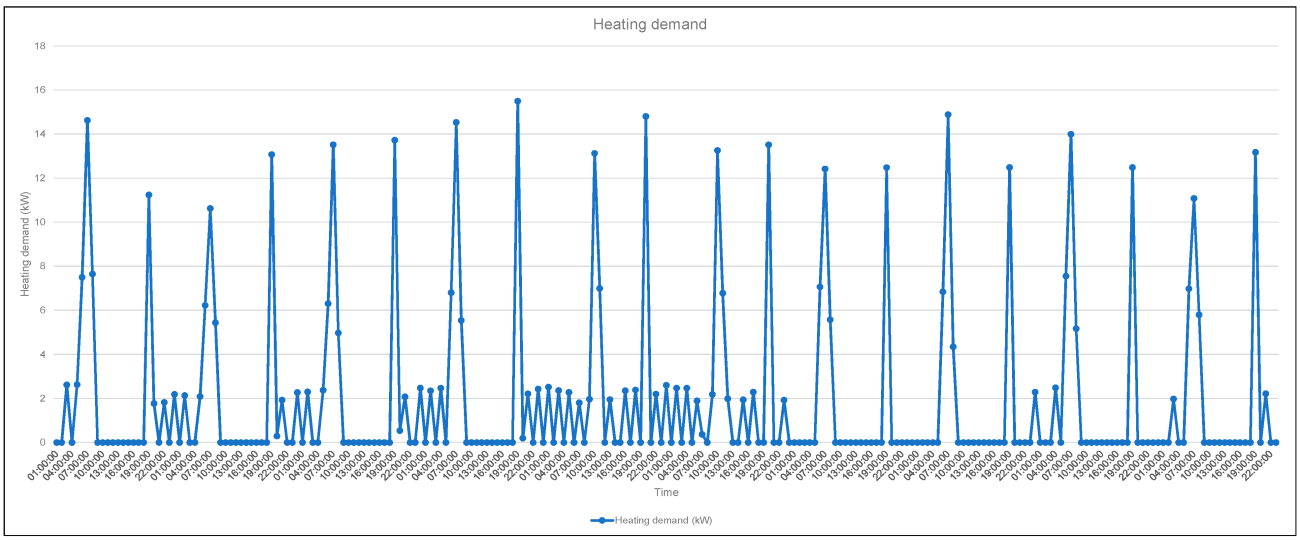

(**a**)

Figure 8 • *Cont.*

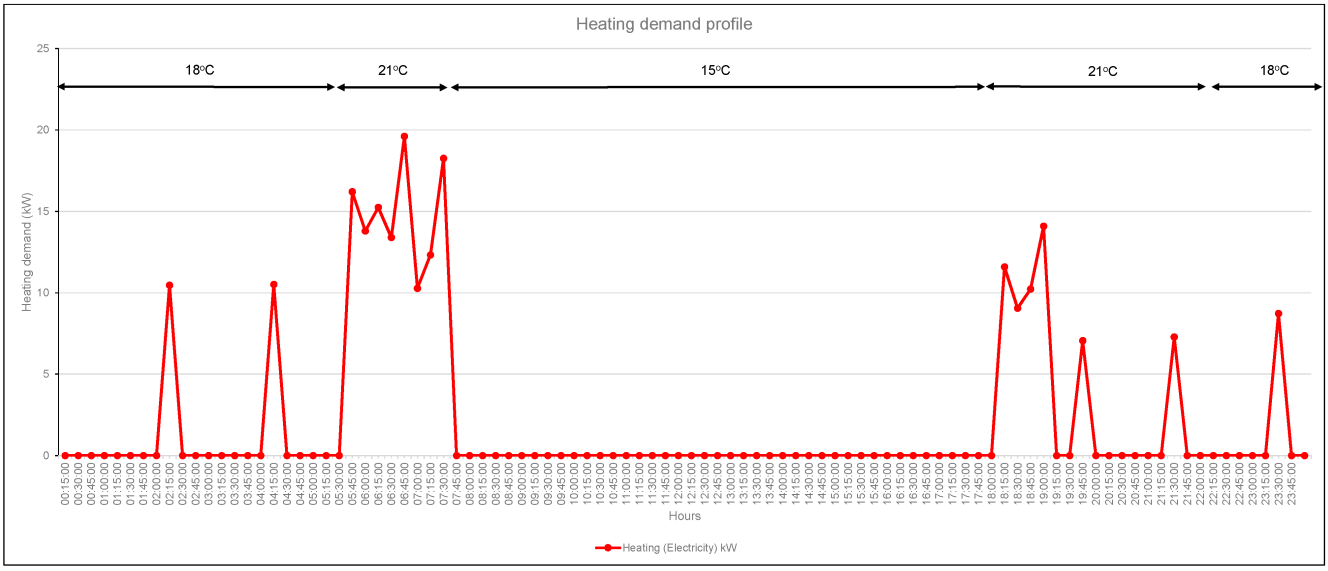

(**b**)

Figure 8 • (**a**) Hourly heating demand profile across a 10-day winter period in the baseline building model; (**b**) hourly heating demand profile for a representative January day in the baseline building model.

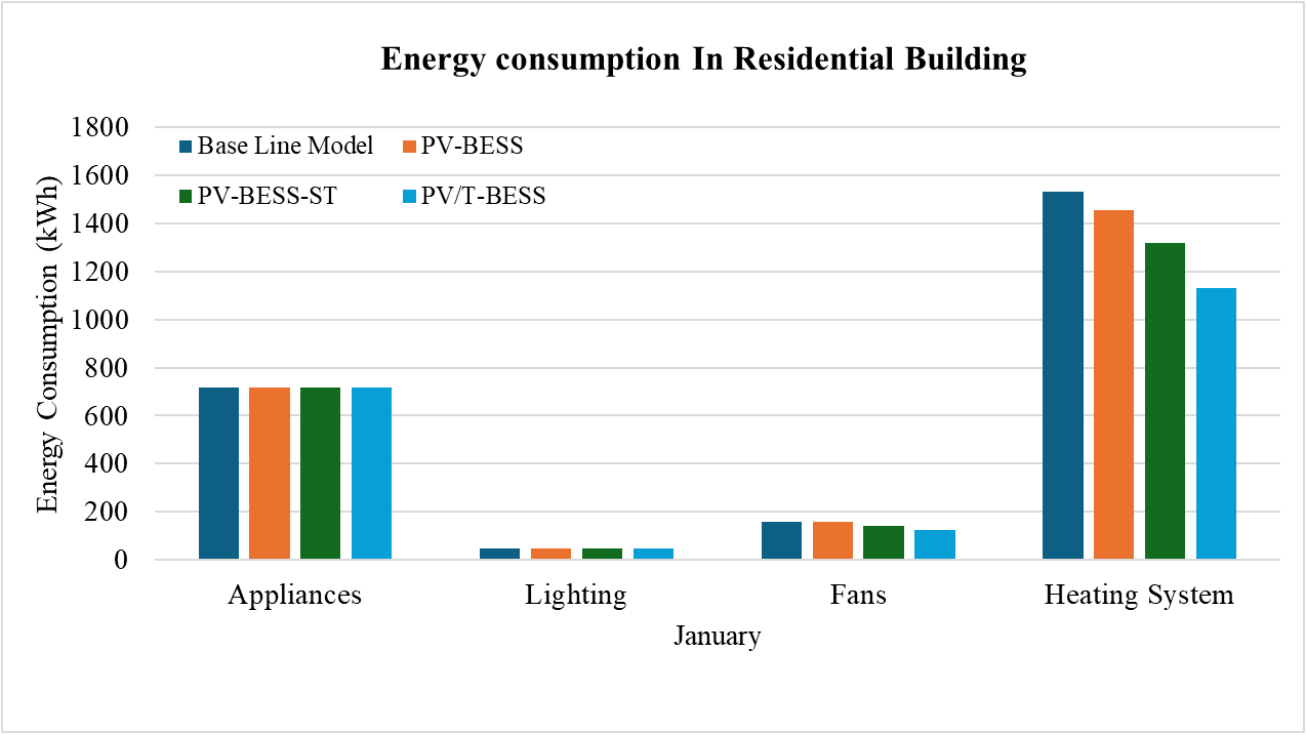

Figure 9 • Electricity consumption in the residential building with integration of different technologies.

In Case 3, a photovoltaic/thermal (PVT) collector was coupled with the BESS, providing simultaneous electrical and thermal generation. This configuration achieved the best overall performance, reducing the peak electricity demand to 9 kW (**Figure 9**) and lowering fan energy use to 123.86 kWh. The total electricity demand of the residential building decreased to 1208.45 kWh and further to 1132.47 kWh when PV generation was utilised (**Figure 9**). Consequently, the overall energy consumption declined to 2019.61 kWh (**Figure 10**), a 17.7% reduction compared with the base case. The superior performance of the PVT–BESS can be attributed to its dual energy recovery mechanism: the thermal component maintains higher inlet temperatures for the ASHP evaporator, thereby improving compressor efficiency, while the electrical component supplies power to the system and charges the battery. The resulting SCOP increased to approximately 4.1, representing a 13–15% improvement over the standalone ASHP. This increase arises from a combination of reduced compressor power consumption and improved heat exchange stability at the evaporator inlet. The stored electrical energy supports heating during low-solar periods, improving reliability and self-sufficiency. These findings align with those of ref. [40], who identified PVT-assisted systems as having the highest exergy efficiency and CO_2 reduction potential among renewable-assisted heat pump systems.

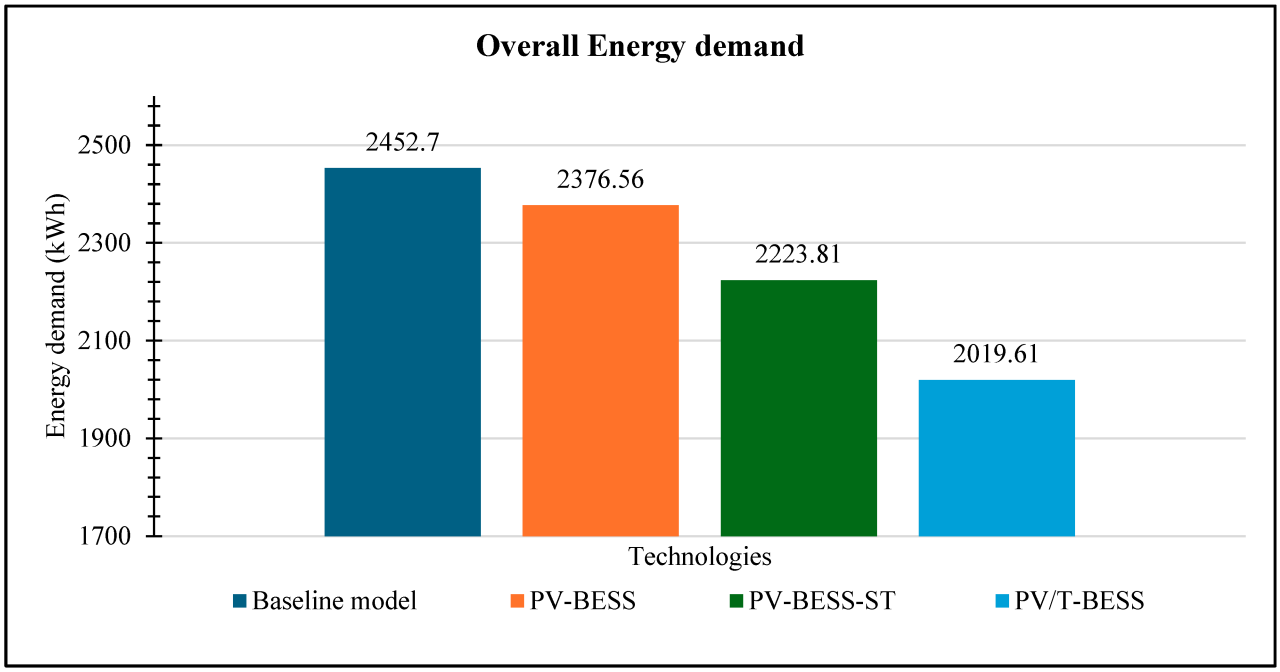

Figure 10 • Overall energy demand of residential buildings during the month of January.

From a 5E framework perspective (Energy, Exergy, Entransy, Economic, and Environmental) as suggested by ref. [11], the PVT–BESS (Case 3) demonstrates the most balanced and sustainable performance. Energetically, it achieves the greatest reduction in energy demand. Exergy analysis highlights more effective utilisation of both electrical and thermal inputs, minimising exergy destruction. Entransy considerations indicate enhanced heat transfer efficiency due to the thermal coupling between PVT and ASHP. Economically, while the PVT system entails higher initial capital cost, its long-term operational savings and emission reductions yield superior lifecycle cost-effectiveness. Environmentally, reduced grid dependency translates into lower indirect CO_2 emissions and improved system sustainability.

Overall, the results show a clear progression: as the degree of system integration increases, the energy and environmental performance improve, though with diminishing marginal gains beyond Case 3. This trend underscores the importance of techno-economic optimisation to balance performance with complexity. While Case 3 offers the best overall outcomes, Case 2 presents a more practical balance between efficiency gains and cost, suggesting it may be more suitable for near-term residential applications. Future work should explore adaptive Energy Management Strategies (EMSs) under varying weather conditions such as representative winter, mid-season, and summer weeks to better capture dynamic system responses and refine control algorithms for year-round optimisation.

4. Conclusions

This study evaluated the effectiveness of integrating different technologies into residential buildings to reduce electricity demand for space heating. The strategies considered include photovoltaic panels with battery energy storage systems (PV–BESS, Case 1), PV–BESS combined with a solar thermal system (Case 2), and a photovoltaic/thermal (PV/T) system coupled with BESS (Case 3). These configurations were compared against a baseline air-source heat pump model (Case 0) to determine their potential for lowering peak electricity loads under cold climatic conditions in the UK. Simulations were conducted for the entire month of January using DesignBuilder/EnergyPlus software to provide a detailed assessment of system performance. Key findings from the analysis are as follows:

- The accuracy of the simulation model was confirmed through close agreement with baseline published results for the David Wilson residential building.
- The thermal and energy performance of the building, when integrated with various technologies, was successfully assessed under cold climate conditions using the developed simulation model.
- In the baseline model (Case 0), the daily electricity heating demand reached 15 kW. This was reduced to 12 kW with the PV–BESS–ST system (Case 2) and further to 9 kW with the PV/T–BESS (Case 3).
- The total electricity demand for January decreased from 1531.6 kWh in Case 0 to 1456.1 kWh with PV–BESS (Case 1), 1318 kWh with PV–BESS–ST (Case 2), and 1132.47 kWh with PV/T–BESS (Case 3).
- Among all configurations, the PV/T–BESS (Case 3) achieved the greatest reduction in both daily peak load and monthly electricity demand for heating.

Additionally, further reductions in electricity demand could be achieved by incorporating thermal energy storage, particularly phase change materials (PCMs), alongside the air-source heat pump. Excess heat generated by the PV/T system could be stored in PCMs during off-peak hours and released during peak periods, improving energy utilisation efficiency and enhancing the operational flexibility of residential heating systems.

Funding

This research received no external funding.

Author contributions

Conceptualization, S.P. and S.T.S.; methodology, S.P. and S.T.S.; software, S.P. and H.S.; validation, S.P. and S.T.S. and H.S.; formal analysis, S.P.; investigation, S.P. and S.T.S.; resources, S.P. and H.S.; data curation, S.P.; writing—original draft preparation, S.P.; writing—review and editing, S.P., S.T.S.; visualisation, S.T.S.; supervision, S.T.S.; project administration, S.T.S. All authors have read and agreed to the published version of the manuscript.

Conflict of interest

The authors declare that they have no competing interests.

Data availability statement

The data supporting the findings of this publication can be made available upon request.

Additional information

Received: 2025-10-01

Accepted: 2025-12-09

Published: 2025-12-22

Academia Green Energy papers should be cited as *Academia Green Energy 2025*, ISSN 2998-3665, https://doi.org/10.20935/AcadEnergy8057. The journal's official abbreviation is *Acad. Energy*.

Publisher's note

Academia.edu Journals stays neutral with regard to jurisdictional claims in published maps and institutional affiliations. All claims expressed in this article are solely those of the authors and do not necessarily represent those of their affiliated organizations, or those of the publisher, the editors and the reviewers. Any product that may be evaluated in this article, or claim that may be made by its manufacturer, is not guaranteed or endorsed by the publisher.

Copyright

References

1. Xia W, Apergis N, Bashir MF, Ghosh S, Doğan B, Shahzad U. Investigating the role of globalization, and energy consumption for environmental externalities: empirical evidence from developed and developing economies. Renew Energy. 2022;183:219–28. doi: 10.1016/j.renene.2021.10.084
2. Preet S, Mathur S, Mathur J, Sharma MK, Chowdhury A. Energy characterization of forced ventilated Photovoltaic-DSF system in hot summer of composite climate. Energy Built Environ. 2023;5(5):704–18. doi: 10.1016/j.enbenv.2023.05.008
3. IEA. World energy outlook 2022. 2022 [accessed on 2025 Dec 3]. Available from: https://www.iea.org/reports/world-energy-outlook-2022
4. Wilberforce T, Olabi AG, Sayed ET, Elsaid K, Maghrabie HM, Abdelkareem MA. A review on zero energy buildings–pros and cons. Energy Built Environ. 2023;4(1):25–38. doi: 10.1016/j.enbenv.2021.06.002
5. Ward WO, Li X, Sun Y, Dai M, Arbabi H, Tingley DD, et al. Estimating energy consumption of residential buildings at scale with drive-by image capture. Build Environ. 2023;234:110188. doi: 10.1016/j.buildenv.2023.110188
6. Von Malmborg F. Exploring advocacy coalitions for energy efficiency: policy change through internal shock and learning in the European Union. Energy Res Soc Sci. 2021;80:102248. doi: 10.1016/j.erss.2021.102248
7. Lamnatou C, Chemisana D, Cristofari C. Smart grids and smart technologies in relation to photovoltaics, storage systems, buildings and the environment. Renew Energy. 2022;185:1376–91. doi: 10.1016/j.renene.2021.11.019
8. Panda S, Mohanty S, Rout PK, Sahu BK, Bajaj M, Zawbaa HM, et al. Residential demand side management model, optimization and future perspective: a review. Energy Rep. 2022;8:3727–66. doi: 10.1016/j.egyr.2022.02.300
9. Dixon J, Bell K, Brush S. Which way to net zero? A comparative analysis of seven UK 2050 decarbonisation pathways. Renew Sustain Energy Transit. 2022;2:100016. doi: 10.1016/j.rset.2021.100016
10. Ramirez-Mendiola JL, Mattioli G, Anable J, Torriti J. I'm coming home (to charge): the relation between commuting practices and peak energy demand in the United Kingdom. Energy Res Soc Sci. 2022;88:102502. doi: 10.1016/j.erss.2022.102502
11. Preet S, Radcliffe J. Heat pump–phase change material systems: a comprehensive review of thermophysical properties and design parameters within a 5E analysis framework. Appl Therm Eng. 2025;128293. doi: 10.1016/j.applthermaleng.2025.128293
12. Uddin M, Romlie MF, Abdullah MF, Abd Halim S, Kwang TC. A review on peak load shaving strategies. Renew Sustain Energy Rev. 2018;82:3323–32. doi: 10.1016/j.rser.2017.10.056
13. Kanakadhurga D, Prabaharan N. Demand side management in microgrid: a critical review of key issues and recent trends. Renew Sustain Energy Rev. 2022;156:111915. doi: 10.1016/j.rser.2021.111915
14. Obi M, Slay T, Bass R. Distributed energy resource aggregation using customer-owned equipment: a review of literature and standards. Energy Rep. 2020;6:2358–69. doi: 10.1016/j.egyr.2020.08.035

15. Pimm AJ, Cockerill TT, Taylor PG. Time-of-use and time-of-export tariffs for home batteries: effects on low voltage distribution networks. J Energy Storage. 2018;18:447–58. doi: 10.1016/j.est.2018.06.008

16. Kutlu C, Tapia-Brito E, Agbonaye O, Su Y, Smith ST, Hughes B, et al. Incorporation of controllable supercooled phase change material heat storage with a solar assisted heat pump: testing of crystallization triggering and heating demand-based modelling study. J Energy Storage. 2022;55:105744. doi: 10.1016/j.est.2022.105744

17. Sezen K, Gungor A. Performance analysis of air source heat pump according to outside temperature and relative humidity with mathematical modeling. Energy Convers Manag. 2022;263:115702. doi: 10.1016/j.enconman.2022.115702

18. Kim T, Choi BI, Han YS, Do KH. A comparative investigation of solar-assisted heat pumps with solar thermal collectors for a hot water supply system. Energy Convers Manag. 2018;172:472–84. doi: 10.1016/j.enconman.2018.07.035

19. Bellos E, Tzivanidis C. Multi-objective optimization of a solar assisted heat pump-driven by hybrid PV. Appl Therm Eng. 2019;149:528–35. doi: 10.1016/j.applthermaleng.2018.12.059

20. Bahman AM, Parikhani T, Ziviani D. Multi-objective optimization of a cold-climate two-stage economized heat pump for residential heating applications. J Build Eng. 2022;46:103799. doi: 10.1016/j.jobe.2021.103799

21. Zhang H, Jiang L, Zheng W, You S, Jiang T, Shao S, et al. Experimental study on a novel thermal storage refrigerant-heated radiator coupled with air source heat pump heating system. Build Environ. 2019;164:106341. doi: 10.1016/j.buildenv.2019.106341

22. Schram WL, Lampropoulos I, van Sark WG. Photovoltaic systems coupled with batteries that are optimally sized for household self-consumption: assessment of peak shaving potential. Appl Energy. 2018;223:69–81. doi: 10.1016/j.apenergy.2018.04.023

23. Leadbetter J, Swan L. Battery storage system for residential electricity peak demand shaving. Energy Build. 2012;55:685–92. doi: 10.1016/j.enbuild.2012.09.035

24. Babacan O, Ratnam EL, Disfani VR, Kleissl J. Distributed energy storage system scheduling considering tariff structure, energy arbitrage and solar PV penetration. Appl Energy. 2017;205:1384–93. doi: 10.1016/j.apenergy.2017.08.025

25. Lokeshgupta B, Sivasubramani S. Multi-objective home energy management with battery energy storage systems. Sustain Cities Soc. 2019;47:101458. doi: 10.1016/j.scs.2019.101458

26. Roberts MB, Bruce A, MacGill I. Impact of shared battery energy storage systems on photovoltaic self-consumption and electricity bills in apartment buildings. Appl Energy. 2019;245:78–95. doi: 10.1016/j.apenergy.2019.04.001

27. Ghadimi N, Sedaghat M, Azar KK, Arandian B, Fathi G, Ghadamyari M. An innovative technique for optimization and sensitivity analysis of a PV/DG/BESS based on converged Henry gas solubility optimizer: a case study. IET Gener Transm Distrib. 2023;17(21):4735–49. doi: 10.1049/gtd2.12773

28. Garg V, Mathur J, Bhatia A. Building energy simulation: a workbook using designbuilder™. Boca Raton (FL): CRC Press; 2020.

29. Martínez-Gracia A, Uche J, del Amo A, Bayod-Rújula ÁA, Usón S, Arauzo I. Energy and environmental benefits of an integrated solar photovoltaic and thermal hybrid, seasonal storage and heat pump system for social housing. Appl Therm Eng. 2022;213:118662. doi: 10.1016/j.applthermaleng.2022.118662

30. Mujeebu MA, Bano F. Energy-saving potential and cost-effectiveness of active energy-efficiency measures for residential building in warm-humid climate. Energy Sustain Dev. 2022;67:163–76. doi: 10.1016/j.esd.2022.01.011

31. Al Huneidi DI, Tahir F, Al-Ghamdi SG. Energy modeling and photovoltaics integration as a mitigation measure for climate change impacts on energy demand. Energy Rep. 2022;8:166–71. doi: 10.1016/j.egyr.2022.01.105

32. Preet S, Mathur S, Mathur J, Smith ST, Saini H. Multivariate optimization of mechanically ventilated photovoltaic double-skin façade system for the cold conditions of composite climate zone. Build Eng. 2025;3(2):1946. doi: 10.59400/be1946

33. Preet S, Sharma MK, Mathur J, Chowdhury A, Mathur S. Analytical model of semi-transparent photovoltaic double-skin façade system (STPV-DSF) for natural and forced ventilation modes. Int J Vent. 2023;22(2):138–67. doi: 10.1080/14733315.2021.1971873

34. Hlanze P, Jiang Z, Cai J, Shen B. Model-based predictive control of multi-stage air-source heat pumps integrated with phase change material-embedded ceilings. Appl Energy. 2023;336:120796. doi: 10.1016/j.apenergy.2023.120796

35. Kim MH, Bullard CW. Thermal performance analysis of small hermetic refrigeration and air-conditioning compressors. JSME Int J Ser B Fluids Therm Eng. 2002;45(4):857–64. doi: 10.1299/jsmeb.45.857

36. Preet S, Smith ST. A comprehensive review on the recycling technology of silicon based photovoltaic solar panels: challenges and future outlook. J Clean Prod. 2024;448:141661. doi: 10.1016/j.jclepro.2024.141661

37. Preet S, Bhushan B, Mahajan T. Experimental investigation of water based photovoltaic/thermal (PV/T) system with and without phase change material (PCM). Sol Energy. 2017;155:1104–20. doi: 10.1016/j.solener.2017.07.040

38. Manivannan R, Vigneswar N. A comprehensive review of fractional-order mathematical models for lithium-ion batteries: historical progress, recent advancements, and future outlooks. J Energy Storage. 2025;131:117404. doi: 10.1016/j.est.2025.117404

39. CIBSE. CIBSE guide a: environmental design. London: CIBSE; 2016 [accessed on 2025 Dec 3]. Available from: https://www.cibse.org/ljmpptci/guide-a-presentation.pdf

40. Olympios AV, Sapin P, Freeman J, Olkis C, Markides CN. Operational optimisation of an air-source heat pump system with thermal energy storage for domestic applications. Energy Convers Manag. 2022;273:116426. doi: 10.1016/j.enconman.2022.116426

41. Xu T, Humire EN, Chiu JN, Sawalha S. Latent heat storage integration into heat pump based heating systems for energy-efficient load shifting. Energy Convers Manag. 2021;236:114042. doi: 10.1016/j.enconman.2021.114042